

Elucidating the Trade-off between Membrane Wetting Resistance and Water Vapor Flux in Membrane Distillation

Chenxi Li, Xuesong Li, Xuewei Du, Ying Zhang, Wei Wang, Tiezheng Tong, Arun K. Kota, and Jongho Lee

Environ. Sci. Technol., **Just Accepted Manuscript** • DOI: 10.1021/acs.est.0c02547 • Publication Date (Web): 23 Jul 2020

Downloaded from pubs.acs.org on July 28, 2020

Just Accepted

“Just Accepted” manuscripts have been peer-reviewed and accepted for publication. They are posted online prior to technical editing, formatting for publication and author proofing. The American Chemical Society provides “Just Accepted” as a service to the research community to expedite the dissemination of scientific material as soon as possible after acceptance. “Just Accepted” manuscripts appear in full in PDF format accompanied by an HTML abstract. “Just Accepted” manuscripts have been fully peer reviewed, but should not be considered the official version of record. They are citable by the Digital Object Identifier (DOI®). “Just Accepted” is an optional service offered to authors. Therefore, the “Just Accepted” Web site may not include all articles that will be published in the journal. After a manuscript is technically edited and formatted, it will be removed from the “Just Accepted” Web site and published as an ASAP article. Note that technical editing may introduce minor changes to the manuscript text and/or graphics which could affect content, and all legal disclaimers and ethical guidelines that apply to the journal pertain. ACS cannot be held responsible for errors or consequences arising from the use of information contained in these “Just Accepted” manuscripts.

27 **ABSTRACT**

28 Membrane distillation (MD) has been receiving considerable attentions as a promising
29 technology for desalinating industrial wastewaters. While hydrophobic membranes are essential
30 for the process, increasing membrane surface hydrophobicity generally leads to the reduction of
31 water vapor flux. In this study, we investigate the mechanisms responsible for this trade-off
32 relation in MD. We prepared hydrophobic membranes with different degrees of wetting
33 resistances through coating quartz fiber membranes with a series of alkylsilane molecules while
34 preserving the fiber structures. A trade-off between wetting resistance and water vapor flux was
35 observed in direct-contact MD experiments, with the least wetting-resistant membrane exhibiting
36 twice as high vapor flux as the most wetting-resistant membrane. Electrochemical impedance
37 analysis, combined with fluorescence microscopy, elucidated that a lower wetting resistance
38 (still water-repelling) allows deeper penetration of liquid-air interfaces into the membrane,
39 resulting in an increased interfacial area and therefore a larger evaporative vapor flux. Finally,
40 we performed osmotic distillation experiments employing anodized alumina membranes that
41 possess straight nanopores with different degrees of wetting resistance, observed no trade-off,
42 and substantiated this proposed mechanism. Our study provides a guideline to tailoring the
43 membrane surface wettability to ensure stable MD operations while maximizing the water
44 recovery rate.

45

46

47

48

49 INTRODUCTION

50 Consuming approximately 20% of global freshwater withdrawal, industrial sector is the second
51 largest consumer of freshwater resources following the agriculture sector.¹ Its rapidly growing
52 freshwater consumption makes water reclamation from industrial wastewaters an important
53 practice in reducing the freshwater demand.² Moreover, the increasingly stringent discharge
54 regulation such as zero liquid discharge also necessitates the efficient water reclamation and
55 reuse from industrial wastewaters.³ A significant fraction of industrial wastewaters such as those
56 generated from manufacturing, mining, oil and gas sectors,⁴ typically contains a variety of
57 contaminants including highly concentrated salts (up to 360,000 ppm), oil, alcohols, and other
58 organic pollutants.^{2,5} As a state-of-the-art membrane separation technology for recovering clean
59 water from industrial wastewaters, reverse osmosis (RO), however, has a treatable salinity limit
60 ($< \sim 70,000 \text{ mg L}^{-1}$) due to the prohibitively high osmotic pressure to overcome, and exhibits
61 unsatisfactory rejection against some specific organic pollutants.^{5,6}

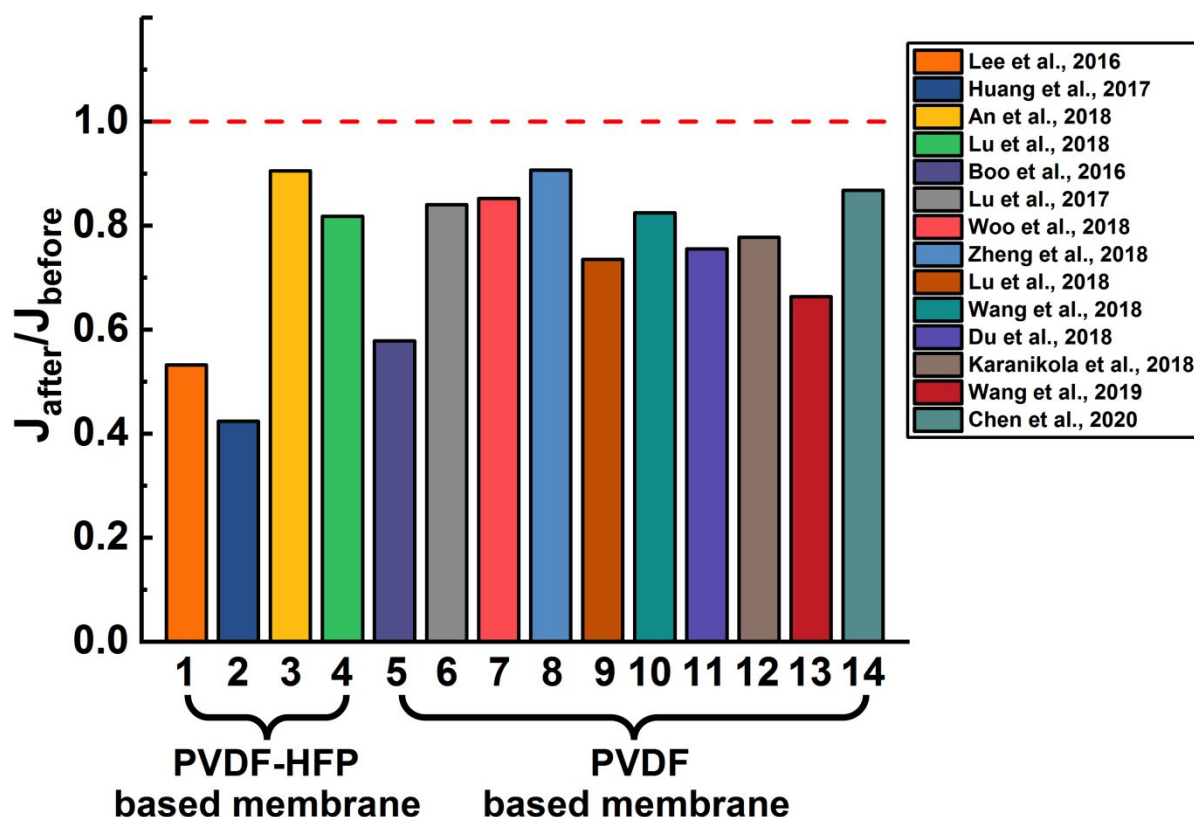
62 Membrane distillation (MD) has attracted considerable attentions in recent years as an
63 alternative process for water reclamation from highly-saline wastewaters.⁷⁻¹² MD is a thermal
64 desalination process, in which water vapor is driven by vapor pressure gradient from a hot feed
65 to a cold permeate across a porous hydrophobic membrane. The phase-change desalination
66 mechanism makes its water flux and energy consumption fairly insensitive to the feed salinity
67 and enables near-complete salt rejection. Like other thermal desalination processes, MD is an
68 energy-intensive process. However, MD can be operated at a moderate temperature, much lower
69 than the boiling point of water, which renders MD a potentially low-energy-cost process if low-
70 grade heat or waste heat is utilized.¹³

71 In MD process, the membrane must resist wetting to keep the feed and permeate separated.¹⁴
72 However, ubiquitous low-surface-tension contaminants in industrial wastewaters, such as oil,
73 alcohols, and surfactants, can increase the risk of membrane pore wetting in the MD
74 operation.^{10,15,16} As such, developing highly wetting-resistant membranes has been extensively
75 investigated, commonly through modifying the membrane surface by grafting low-surface-
76 energy materials and/or creating a re-entrant structure to the extent that the membrane becomes
77 omniphobic (i.e., resisting low-surface-tension liquids).¹⁷⁻²²

78 While those modified membranes exhibited excellent wetting resistance, a noticeable
79 reduction of MD water vapor flux has been observed in many experiments. Figure 1 shows a
80 summary of MD water flux changes in recent publications (detailed data shown in Table S1),⁸⁻
81 ^{10,19,23-32} as a result of surface modifications of hydrophobic membranes made of poly(vinylidene
82 fluoride) (PVDF) or poly(vinylidene fluoride-co-hexafluoropropylene) (PVDF-HFP) with low-
83 surface-energy materials. Lower water vapor fluxes were observed after the modifications
84 ($J_{\text{after}}/J_{\text{before}} < 1$) in all surveyed cases, though a few exceptions were also reported.³³⁻³⁵ While
85 MD water flux is significantly influenced by membrane structures,¹³ detailed information on the
86 change in thickness, porosity, and pore size after such modifications is rarely available in the
87 literature (summarized in Table S1), making it difficult to examine the sole impact of wetting
88 resistance on water flux.

89 In a very recent study, this trade-off relation between wetting resistance and water vapor flux
90 has been investigated using PVDF-based membranes with different wettabilities.³¹ It was
91 suggested that a membrane with a lower wetting resistance (but still water-repelling) has a larger
92 number of partially wetted pores, leading to a higher liquid-air interfacial area and thus a higher
93 water vapor flux. While this hypothesis was supported by the numerical simulations of dynamic

94 liquid-air interface formation, further experimental verification is necessary to thoroughly
 95 substantiate and validate this hypothesis. In addition, while PVDF membranes of irregular
 96 structures were used in the study, generalization of this hypothesis to other types of membranes
 97 warrants further investigation. Since an enhanced wetting resistance at the expense of water
 98 vapor flux may cause a reduced efficiency of MD process for water reclamation, it is of great
 99 importance to elucidate the underlying mechanism of such a trade-off relation, which will be
 100 critical to guarantee a stable MD operation without compromising the water vapor flux.



101
 102 **Figure 1.** Ratios of water flux after the surface modification of PVDF or PVDF-HFP based membrane
 103 with low-surface-energy materials (J_{after}) to water flux before the modification (J_{before}), calculated from the
 104 data in the literature of direct-contact membrane distillation (DCMD). PVDF stands for poly(vinylidene
 105 fluoride) and PVDF-HFP stands for poly(vinylidene fluoride-co-hexafluoropropylene).

106

107 In this work, we elucidate the underlying mechanism for the trade-off relation between the
108 membrane wetting resistance and water vapor flux in MD. We modify a fibrous membrane with
109 a series of low-surface-energy alkylsilane molecules to fabricate hydrophobic/omniphobic
110 membranes that possess varying degrees of wetting resistance while maintaining identical
111 membrane structures and morphologies. We confirm the trade-off relation in direct-contact
112 membrane distillation (DCMD) experiments with the fabricated membranes. We examine the
113 impact of membrane thermal conductance, air-gap distance in the membrane, and liquid-air
114 interfacial area on the water flux using various techniques including thermal conductivity
115 measurement, fluorescence microscopy, and electrochemical impedance spectroscopy (EIS).
116 Further, we perform osmotic distillation (OD) experiments using porous alumina membranes that
117 comprise straight nanopores, which exhibit different wettabilities but possess identical liquid-air
118 interfacial areas available for water evaporation and condensation. Taken together, we identify
119 the determining factor for the trade-off relation and propose potential mechanisms. Our findings
120 can serve as a guideline for membrane fabrications suitable for MD in various industrial
121 applications.

122

123 **MATERIALS AND METHODS**

124 **Materials and Chemicals.** Quartz fiber (QF) membranes (membrane type: QR-100) with an
125 average thickness of 0.38 mm were supplied by Sterlitech (WA, USA). This type of QF
126 membrane retains 99.99% of dioctylphthalate-derived particles having a diameter of 0.3 μm
127 (data provided by the supplier) and the porosity of QR-100 is $79.3 \pm 1.3\%$ determined by the
128 pycnometric method.³⁶ Nanoporous anodized aluminum oxide (AAO) membranes with the
129 nominal diameter of 200 nm and porosity of approximately 10 % were supplied by InRedox

130 (CO, USA). Four silane agents were selected for the surface silanization of QF membranes and
131 AAO membranes: trimethoxy(propyl)silane (AS, 97%, Sigma-Aldrich), (3,3,3-
132 trifluoropropyl)trimethoxysilane (FAS-3, 98%, Gelest Inc.), nonafluorohexyltriethoxysilane
133 (FAS-9, 98%, Gelest Inc.), and 1H,1H,2H,2H-perfluorodecyltriethoxysilane (FAS-17, 98%,
134 Gelest Inc.). N,N-dimethylformamide (DMF, 99.8%) was purchased from VWR International.
135 Hexadecane ($\geq 98\%$), sodium chloride (NaCl, $\geq 99\%$), and sodium dodecyl sulfate (SDS) were
136 obtained from Fisher Scientific. Distilled water was generated by a Synergy[®] UV water
137 purification system (Millipore, Billerica, MA). The other chemicals were supplied by Sigma-
138 Aldrich unless otherwise stated.

139 **Fabrication of Hydrophobic Membranes with Different Wetting Resistances.** The
140 hydrophobic modification processes of QF and AAO membranes were schematically illustrated
141 in Figure S1. The pristine QF membrane was immersed in a DMF solution containing 3.5 wt%
142 poly(vinylidene fluoride-co-hexafluoropropylene) (PVDF-HFP, $M_w \sim 400,000$) and 1% v/v
143 silane (i.e., AS, FAS-3, FAS-9, and FAS-17) for 2 hours under a continuous shaking, which was
144 subsequently placed in an oven at 105 °C for 4 hours to completely remove DMF. The modified
145 QF membrane was subjected to a hot-press treatment under 0.5 bar at 160 °C for 1 hour to
146 enhance its compactness. The hydrophobic AAO membranes were fabricated by soaking the
147 pristine membrane in a hexane solution containing 1% v/v silane (i.e., AS, FAS-3, FAS-9, and
148 FAS-17) for 20 hours, followed by a heat-treatment at 105 °C for 4 hours after a thorough rinse
149 with hexane.

150 **Membrane Characterizations.** The surface morphologies and cross-section structures of
151 modified membranes were characterized using a scanning electron microscope (SEM, FEI
152 Quanta 650). The surface wettabilities were characterized by measuring the static contact angles

153 of different liquids using a goniometer (Ramé-Hart 200-F1). Thermal conductivities of
 154 membranes were assessed by using a thermal conductivity analyzer (Hot Disk TPS 2500S)
 155 equipped with a thin film sensor with a nickel double spiral insulated in a thin layer of Kapton.
 156 For the thermal conductivity analysis, twenty membrane samples with the same size were
 157 stacked and placed on each side of the sensor, which were compressed under a fixed pressure
 158 (0.6 bar).

159 Silicon wafers were used to assess the surface energies of different silanes. Prior to the
 160 surface silanization, the silicon wafer was first cleaned with a piranha solution (3:1 v/v sulfuric
 161 acid : hydrogen peroxide mixture) for 2 hours, followed by a thorough rinse with distilled water.
 162 After rinsing, the silicon wafer was dried at 105 °C for 2 hours. The silanization of the cleaned
 163 silicon wafer was performed following the same protocol as that used for AAO membrane
 164 modification. The method proposed by Wu³⁷ was used to calculate the surface energy of a silane-
 165 modified surface as it is suitable for analyzing the surface with a relatively low surface energy.³⁸
 166 The total surface energy (γ_{sv}) may be decomposed into dispersion (γ_{sv}^d) and polar components
 167 (γ_{sv}^p):

$$\gamma_{sv} = \gamma_{sv}^d + \gamma_{sv}^p \quad (1.)$$

168 By measuring the static contact angles of water (θ_{water}) and diiodomethane (θ_{D-M}) on modified
 169 silicon wafers, γ_{sv}^d and γ_{sv}^p can be calculated by using the following equations:

$$[1 + \cos(\theta_{water})]\gamma_{water} = 4 \left(\frac{\gamma_{water}^d \cdot \gamma_{sv}^d}{\gamma_{water}^d + \gamma_{sv}^d} + \frac{\gamma_{water}^p \cdot \gamma_{sv}^p}{\gamma_{water}^p + \gamma_{sv}^p} \right) \quad (2.)$$

$$[1 + \cos(\theta_{D-M})]\gamma_{D-M} = 4 \left(\frac{\gamma_{D-M}^d \cdot \gamma_{sv}^d}{\gamma_{D-M}^d + \gamma_{sv}^d} + \frac{\gamma_{D-M}^p \cdot \gamma_{sv}^p}{\gamma_{D-M}^p + \gamma_{sv}^p} \right) \quad (3.)$$

170 The dispersive components of water (γ_{water}^d) and diiodomethane (γ_{D-M}^d) are 21.8 mN·m⁻¹
171 and 49.5 mN·m⁻¹, respectively, while the polar components of water (γ_{water}^p) and diiodomethane
172 (γ_{D-M}^p) are 51.0 mN·m⁻¹ and 1.3 mN·m⁻¹, respectively.³⁹

173 The protrusion of liquid-air interfaces into the membrane pores was assessed via
174 electrochemical impedance spectroscopy (EIS). The modified QF membrane was mounted in a
175 cross-flow membrane cell having an effective area of 3 cm² (12 mm × 25 mm). Each channel
176 oilkwas filled with the electrolyte solution (1 M NaCl solution with different concentrations of
177 SDS). A titanium sheet was inserted into each flow channel to directly contact the membrane,
178 and the other end was connected to a potentiostat (Interface 1010E, Gamry Instruments) with a
179 built-in software to monitor the impedance of the system. The frequency was varied from 10³ Hz
180 to 10⁶ Hz. The detailed procedure to estimate the effective capacitance from EIS measurements
181 is described in the Supporting Information Section 1.

182 The degree of penetration of feed water into the membranes was visualized via fluorescence
183 microscopy. The modified QF membrane was assembled in a dead-end filtration cell which was
184 filled with an aqueous solution containing 0.01 mg/mL Rhodamine B and 0.01 mM SDS ($\gamma \approx 66$
185 mN·m⁻¹, the same surface tension as the feed water at 60 °C) for 0.5 hour. The height of the
186 liquid solution in the dead-end cell was 10 cm and the hydraulic pressure applied on the
187 membrane was approximately 1 kPa, simulating the hydraulic pressure in the feed channel of the
188 membrane cell during DCMD tests. After staining, the membrane sample was trimmed with
189 blades and visualized by an upright configuration wide field microscope (Olympus BX53).

190 **DCMD Experiments of Modified Membranes.** Water vapor fluxes across the modified QF
191 membranes were measured by a bench-scale DCMD unit with a cross-flow membrane cell with
192 an effective membrane area of 15 cm² (60 mm × 25 mm). NaCl solution (0.5 M) at 60 °C and

193 distilled water at 20 °C were used as the feed and permeate solutions, respectively, whose
194 temperatures were maintained by using two recirculating water baths (Polystat Standard, Cole-
195 Parmer). The feed had a slightly higher crossflow velocity (5.6 cm/s) than the permeate (3.7
196 cm/s), which caused a higher pressure in the feed side than in the permeate side and therefore
197 allowed for an explicit detection of membrane pore wetting. Details on measuring the water
198 vapor flux and salt rejection are described in the Supporting Information Section 2 as well as in
199 our previous publication.²⁰

200 **Osmotic Distillation (OD) Experiments of Modified Membranes.** Water vapor fluxes
201 across the modified AAO membranes under isothermal condition were assessed by a bench-scale
202 OD setup used in our previous studies.^{40,41} The OD setup comprises two chambers that were
203 filled with deionized water (feed) and 4 M NaCl solution (draw), respectively, with the silane-
204 modified AAO membrane mounted in between. The effective membrane area was 28.3 mm²
205 (diameter is 6 mm). The temperature of the entire OD setup was kept constant at 40 °C by using
206 a water jacket circulated from an external temperature-controlled water bath (Polystat Standard,
207 Cole-Parmer). Magnetic stir bars were used to facilitate the mixing of liquid bulk and minimize
208 concentration polarization.

209 The conductivity of the feed solution was monitored using a conductivity probe (isoPod,
210 eDAQ, CO, USA) and a Matlab-coded program to detect salt leakage. The volume change of the
211 draw solution was determined through a glass syringe (Hamilton Company, NV, USA, 250 µL
212 volume, accuracy of ±2.5 µL) that was connected to the draw solution chamber. The water flux,
213 J_w (L m⁻² h⁻¹), through the membrane was calculated from the rate of volume change of water in
214 the syringe.

215

216 **RESULTS AND DISCUSSION**

217 **Enhancing wetting resistance of hydrophobic membranes leads to a lower water**

218 **vapor flux in DCMD.** Investigating the impact of surface wettability on water vapor flux in

219 DCMD requires us to fabricate a series of membranes with different surface wettabilities but

220 having nearly identical membrane structures. Accordingly, all pristine QF membranes were

221 modified following the same protocol except the type of silane molecules used. SEM

222 micrographs in Figure 2a and 2b depict the surface morphology of two QF membranes modified

223 with AS (AS QF membrane) and FAS-17 (FAS-17 QF membrane), respectively. SEM images of

224 other modified QF membranes are also available in Figure S2. The resembled structures and

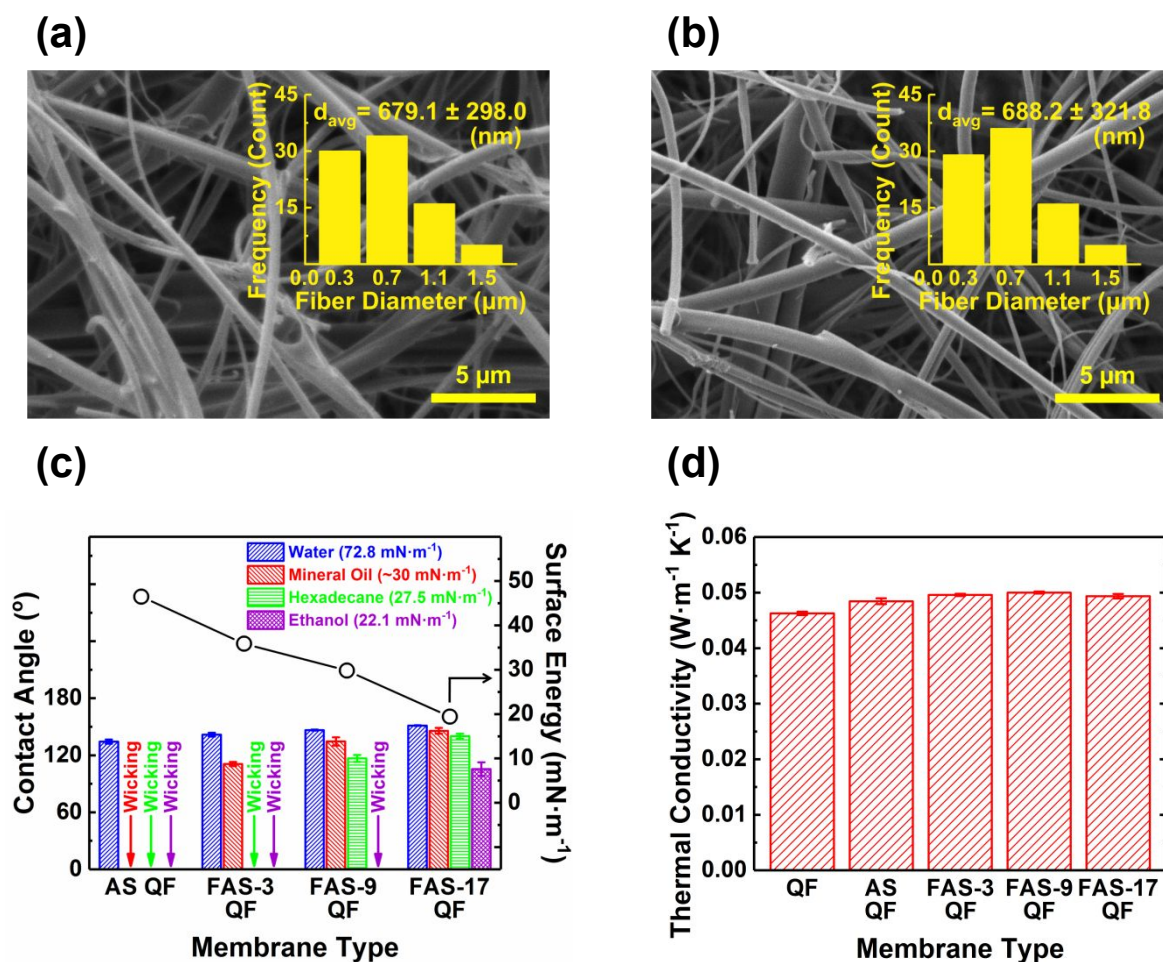
225 similar fiber diameter distributions in modified membranes suggest that the modification with

226 PVDF-HFP/silanes had little effect on the structure of the QF membrane. The variations of

227 thickness, pore size, and porosity in all modified QF membranes were also insignificant (Table

228 S2).

229

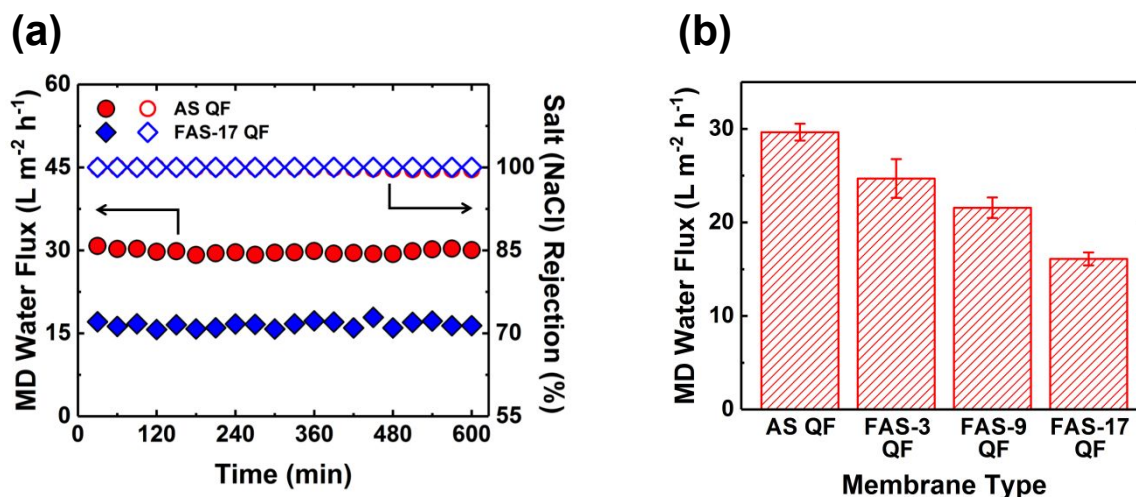


230 **Figure 2.** Characteristics of pristine and modified quartz fiber (QF) membranes. SEM micrographs of the
 231 morphologies of (a) AS QF and (b) FAS-17 QF membranes. The insets are fiber diameter distributions for
 232 each membrane sample. The average diameters (d_{avg}) of fibers in AS QF and FAS-17 QF membranes are
 233 679.1 ± 298.0 nm and 688.2 ± 321.8 nm, respectively. (c) Static contact angles of four different testing
 234 liquids (water, mineral oil, hexadecane, and ethanol) on the surface of the AS QF, FAS-3 QF, FAS-9 QF,
 235 and FAS-17 QF membranes (bar chart). Black circles show the surface energies of the silane-modified
 236 silicon wafer surfaces, calculated from Eqs. (1) – (3). “Wicking” means that the membrane was wetted by
 237 testing liquid droplet, and no stable contact angle could be acquired. Error bars represent the standard
 238 deviations from three different membrane samples (both left and right contact angles were measured on
 239 each sample). (d) Thermal conductivities of the pristine QF membrane and modified QF membranes.
 240 Error bars represent the standard deviations from at least five measurements.

241

242 The different carbon chain lengths and fluorine contents of the four silanes impart the QF
243 membranes with different degrees of hydrophobicity. We used the method proposed by Wu³⁷ to
244 estimate the surface energies of atomically smooth silicon wafers which were coated with the
245 four silanes (Figure 2c). As expected, the estimated surface energy decreases in the order of AS,
246 FAS-3, FAS-9, and FAS-17 modified silicon wafers, and these values agree well with previously
247 reported values in the literature.³⁹ The wettabilities of the modified QF membranes were assessed
248 by measuring static contact angles of several liquids having different surface tensions (γ): water
249 ($\gamma = 72.8 \text{ mN}\cdot\text{m}^{-1}$), mineral oil ($\sim 30 \text{ mN}\cdot\text{m}^{-1}$), hexadecane ($27.5 \text{ mN}\cdot\text{m}^{-1}$), and ethanol (22.1
250 $\text{mN}\cdot\text{m}^{-1}$). All modified QF membranes exhibited water contact angles greater than 130° ,
251 indicating appropriate surface hydrophobicity for MD (Figure 2c). However, the membrane
252 modified with a lower-surface-energy silane retained a lower-surface-tension liquid on its
253 surface without being wetted. As two extreme cases, the FAS-17 QF membrane retained the all
254 testing liquids and exhibited the highest liquid entry pressure (Table S2), while the AS QF
255 membrane only repelled water (the lowest liquid entry pressure, Table S2) and was readily
256 wetted by organic liquids.

257 Water vapor flux in MD is substantially impacted by thermal conductivity of the
258 membrane.¹⁴ A low thermal conductivity is desired for MD in order to establish a steep
259 temperature gradient across the membrane and therefore provides a large driving force for water
260 vapor transport. We measured thermal conductivities of the four differently modified QF
261 membranes using a thermal conductivity meter. Likely due to the negligible mass fraction of
262 coated silanes to the QF substrate, the measured thermal conductivities for the all membranes
263 have very similar values (Figure 2d, $\sim 0.05 \text{ W}\cdot\text{m}^{-1}\cdot\text{K}^{-1}$), from which we anticipate that the thermal
264 conductivity would have little impact on water vapor flux in our DCMD experiments.



265 **Figure 3.** DCMD performance of modified QF membranes. (a) Water vapor flux and salt rejection of the
 266 AS QF (circle symbols) and FAS-17 QF (diamond symbols) membranes in DCMD tests. (b) DCMD
 267 water vapor fluxes of AS QF, FAS-3 QF, FAS-9 QF, and FAS-17 QF membranes. Error bars represent
 268 the standard deviations from three different membrane samples. All DCMD tests were conducted by
 269 using 0.5 M NaCl at 60 °C as the feed solution and distilled water at 20 °C as the permeate solution.

270
 271 The water vapor fluxes for the four differently modified QF membranes were measured in a
 272 lab-scale DCMD setup. Figure 3a shows the time traces of water flux and salt rejection of the AS
 273 QF and FAS-17 QF membranes. Time traces of water fluxes of all four membranes are available
 274 in Figure S3. Here, 0.5 M NaCl solution (60 °C) was used as a feed and distilled water (20 °C) as
 275 a permeate. Both membranes maintained stable water fluxes and nearly perfect salt rejections
 276 (>99%) over 10-hour tests. Noticeably, the water vapor flux of AS QF membrane was
 277 approximately 30 L·m⁻²·h⁻¹, nearly twice as high as that of the FAS-17 QF membrane. Combined
 278 with the FAS-3 QF and FAS-9 QF membranes, also with the nearly perfect salt rejections, a
 279 monotonic decrease of water vapor flux was observed as the wetting resistance of the modified
 280 QF membrane increases (Figure 3b). Since all modified QF membranes exhibited similar
 281 membrane structures and thermal conductivities (Figure 2), we exclude the possibility that this
 282 trend in water flux was caused by any alteration of membrane structures or thermal properties.

283 As such, our results corroborate the previously observed trade-off between membrane wetting
284 resistance and water vapor flux in the MD process.³¹ This observation directs us to investigate
285 the mechanism, as explored in the following sections.

286

287 **The membrane with a higher wetting resistance has a smaller liquid-air interfacial**

288 **area.** Assuming identical membrane structures and thermal conductivities, supported by the

289 previous results, the different water vapor fluxes in DCMD tests may be attributed to potential

290 differences in: (1) liquid-air interfacial areas available for evaporation and condensation, and/or

291 (2) the actual gap distance between the two membrane-solution interfaces across the membrane

292 (i.e., effective membrane thickness). We first applied EIS to examine the differences in these two

293 attributes of the modified QF membranes used in the DCMD process. EIS has been recently

294 implemented to probe the wetting state of hydrophobic membranes in MD process.⁴² Placed

295 between electrolyte solutions (1 M NaCl), a hydrophobic membrane with trapped air may be

296 modeled as a parallel circuit of a resistor and a capacitor when measuring its electrical

297 impedance (Figure 4a).⁴² The high ionic strength of the electrolyte solutions renders the solution

298 impedance negligibly small compared to the membrane impedance (Figure S4). Therefore, we

299 attribute the measured impedance to the membrane only. Based on this simple resistor-capacitor

300 circuit model, we determined the equivalent capacitance of the air-filled hydrophobic membrane

301 via EIS, which is correlated with the liquid-air interfacial area and effective membrane

302 thickness.^{42,43} Taking an air-filled hydrophobic membrane enclosed by the electrolyte as an ideal

303 capacitor, its capacitance can be expressed as:⁴⁴

$$C = \varepsilon_o \varepsilon_m \frac{A_{eff}}{d_{eff}} \quad (4.)$$

304 where ϵ_0 is the permittivity of air (or vacuum) and ϵ_m is the relative permittivity of membrane-air
305 matrix. The value of ϵ_m can be estimated by assuming the matrix as a homogeneous composite
306 material of silica and air, but we obviate the need to calculate ϵ_m by normalizing capacitances to
307 a reference value (Figure 4b). A_{eff} is the effective liquid-air interfacial area and d_{eff} is the
308 effective thickness of the unwetted membrane (i.e. the distance between two liquid-air
309 interfaces). Detailed procedure for estimating the capacitance from EIS is available in the
310 Supporting Information Section 1.

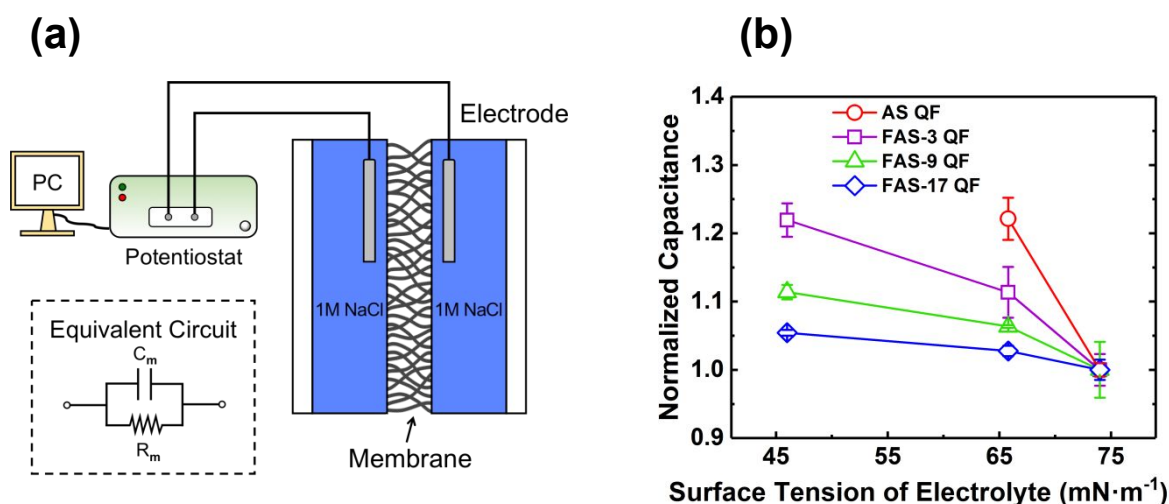
311 If membrane pores are partially wetted, the penetration of the solution into pores can increase
312 the liquid-air interfacial area (A_{eff}) and/or decrease the effective membrane thickness (d_{eff}),
313 resulting in an increased capacitance (C). If the membrane pores are fully wetted, the membrane
314 is equivalent to a resistor with negligible resistance, which can essentially be represented as a
315 short circuit, leading to a drastically reduced overall impedance (Figure S4).

316 In our DCMD tests, the feed (0.5 M NaCl solution) temperature was 60 °C at which its
317 surface tension becomes $\sim 66 \text{ mN}\cdot\text{m}^{-1}$, lower than that of water at 25 °C ($72 \text{ mN}\cdot\text{m}^{-1}$).⁴⁵ To
318 simulate this reduced-surface-tension of the feed in our EIS measurement, we added surfactant
319 (sodium dodecyl sulfate, SDS) into the electrolyte (1 M NaCl solution) to reduce its surface
320 tension to $66 \text{ mN}\cdot\text{m}^{-1}$ and also to $46 \text{ mN}\cdot\text{m}^{-1}$. The Bode plots indicated that all modified QF
321 membranes were in a nonwetted or partially wetted state during EIS measurements, except that
322 AS QF membrane was fully wetted and therefore the measurement was not possible when the
323 surface tension of the electrolyte was reduced to $46 \text{ mN}\cdot\text{m}^{-1}$ (Figure S4). When measured with a
324 surfactant-free electrolyte, FAS-17 QF membrane showed a much lower capacitance than the
325 other membranes (Figure S5), probably because its exceptionally high water repellency does not

326 allow the electrolyte to be in contact to the membrane surface and prevents the penetration of
 327 liquid into membrane pores.

328 Figure 4b shows the normalized capacitances of modified QF membranes after progressively
 329 adding SDS into the electrolyte. Reducing the surface tension of electrolyte is well-correlated
 330 with an increase of the equivalent capacitances for all modified membranes, suggesting that the
 331 membrane exposed to a lower-surface-tension liquid attains a higher liquid-air interfacial area or
 332 a lower effective membrane thickness, or both, which we attribute to the progression of liquid-air
 333 interface into membrane pores. The interface progression into the membrane pores seems to be
 334 more prominent for the membrane having a lower wetting resistance, congruent with the higher
 335 increment of capacitance for the less wetting-resistant membrane.

336



337 **Figure 4.** (a) Schematic illustration of the EIS system used for measuring the impedance of modified QF
 338 membranes. (b) Capacitances of the modified QF membranes estimated from the impedance
 339 measurements using 1 M NaCl solution with different surface tensions (SDS added) as the electrolyte
 340 solution. For each membrane sample, the capacitances were normalized to that with 1 M NaCl with no-
 341 added SDS. Error bars represent the standard deviations from three different membrane samples.

342

343 Next, we employed fluorescence microscopy to investigate the penetration of liquid into the
344 membrane. We selected FAS-9 QF and AS QF membranes due to their distinctly different
345 wettabilities. The top surfaces of both membranes were stained by an aqueous solution
346 containing 0.01 mg/mL Rhodamine B and 0.01 mM SDS under a hydraulic pressure of 1 kPa,
347 simulating the feed surface tension ($\gamma \approx 66 \text{ mN}\cdot\text{m}^{-1}$) and the hydraulic pressure applied on the
348 membrane in our DCMD experiments.

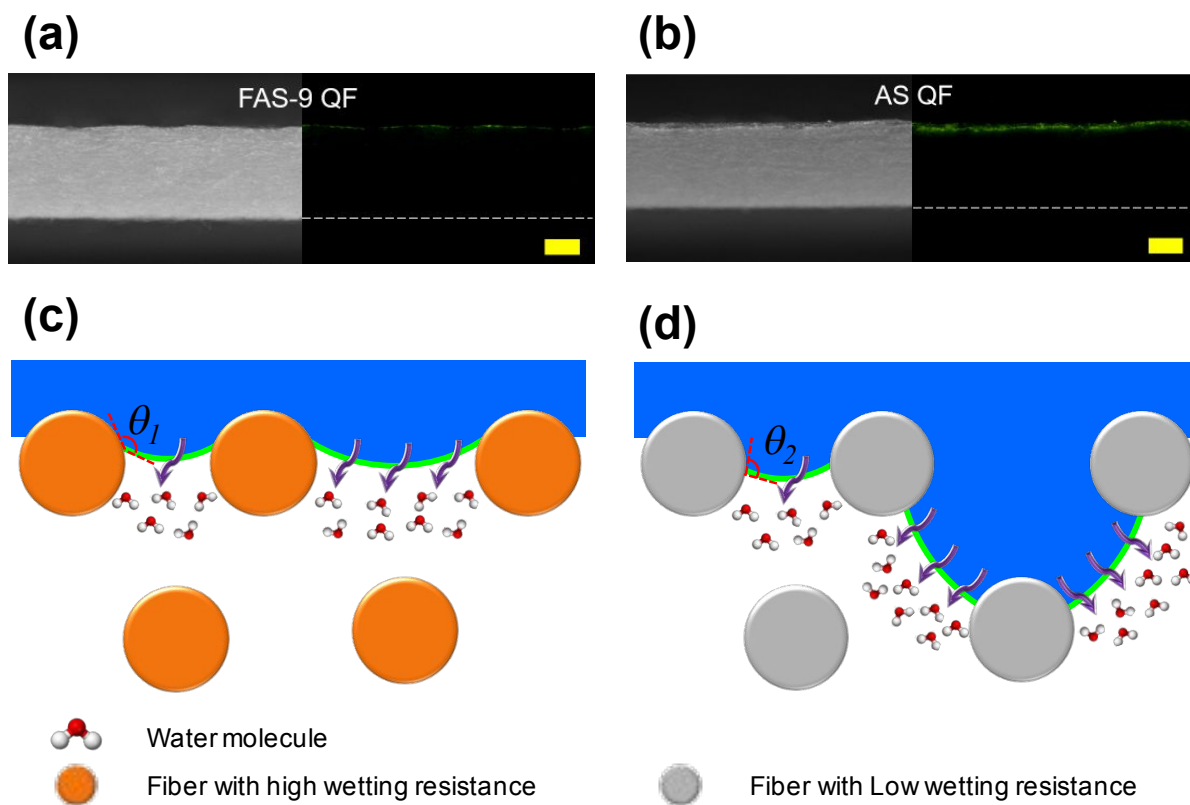
349 Figure 5 visualizes the extent of the penetration of the aqueous dye into the two membranes.
350 The thin bright strips observed on the upper edge of both membranes qualitatively showed that
351 the liquid-air interface did not penetrate into the membrane, which implies that the gap distance
352 between the two interfaces remained to be the membrane thickness during the DCMD
353 experiments for both membranes. The observed maximum strip thickness of AS QF membrane
354 ($\sim 30 \mu\text{m}$) was greater than that of FAS-9 QF membrane ($\sim 10 \mu\text{m}$). Even these maximum
355 thicknesses of the dye strips only accounted for a very small fraction of the entire membrane
356 thickness (less than 6% even for AS QF membrane). The effective thickness (the thickness of
357 nonwetted part) of the AS QF membrane was only approximately 4% lower than that of FAS-9
358 QF membrane. This difference is substantially smaller than the difference between the equivalent
359 capacitances (15%) for AS QF and FAS-9 QF membranes which were determined using EIS
360 with the electrolyte of a surface tension of $66 \text{ mN}\cdot\text{m}^{-1}$ (Figure 4b). Since the equivalent
361 capacitance can be expressed using the interfacial area (A_{eff}) and effective thickness (d_{eff}), given a
362 certain type of membrane (Eq. 4), we conclude that the trade-off between wetting resistance and
363 water vapor flux (Figure 3b) mainly stems from the differences of liquid-air interfacial area.

364 Figure 5c and 5d illustrate potential mechanisms on how the liquid-air interfacial area can be
365 changed by membrane wettability. For the membrane having a high wetting resistance (Figure

366 5c), the intrinsically high contact angle at the cylindrical fiber surface prevents water penetration
367 into membrane pores. The cross-section of cylindrical fibers features re-entrant curvature
368 structure. Therefore, when the wetting resistance is reduced, the fiber network allows liquid-air
369 interface to be formed at the bottom side of the fibers in order to maximize the surface tension
370 forces that resists the wetting front progression.^{39,46,47} The formation of sagging liquid-air
371 interfaces, in particular for fibers with a large interspacing, can induce the contact of the
372 interface to the fiber surface in the subsequent layer, which results in a larger liquid-air
373 interfacial area available for water evaporation and thereby allows for a higher water vapor flux
374 (Figure 5d). This illustration is congruent with the larger thickness of fluorescence dye layer
375 (Figure 5a and 5b) and the greater dependency of the effective capacitance change on the surface
376 tension for the less wetting-resistant membrane (Figure 4b).

377 We note that a more penetration of liquid into the membrane pores can cause a more severe
378 temperature polarization and lead to a reduced water vapor flux.¹⁵ However, Figure 5a and 5b
379 suggest that the water penetration in our membranes is marginal. In such case, the flux
380 enhancement caused by the increased liquid-air interfacial area would dominate.

381



382

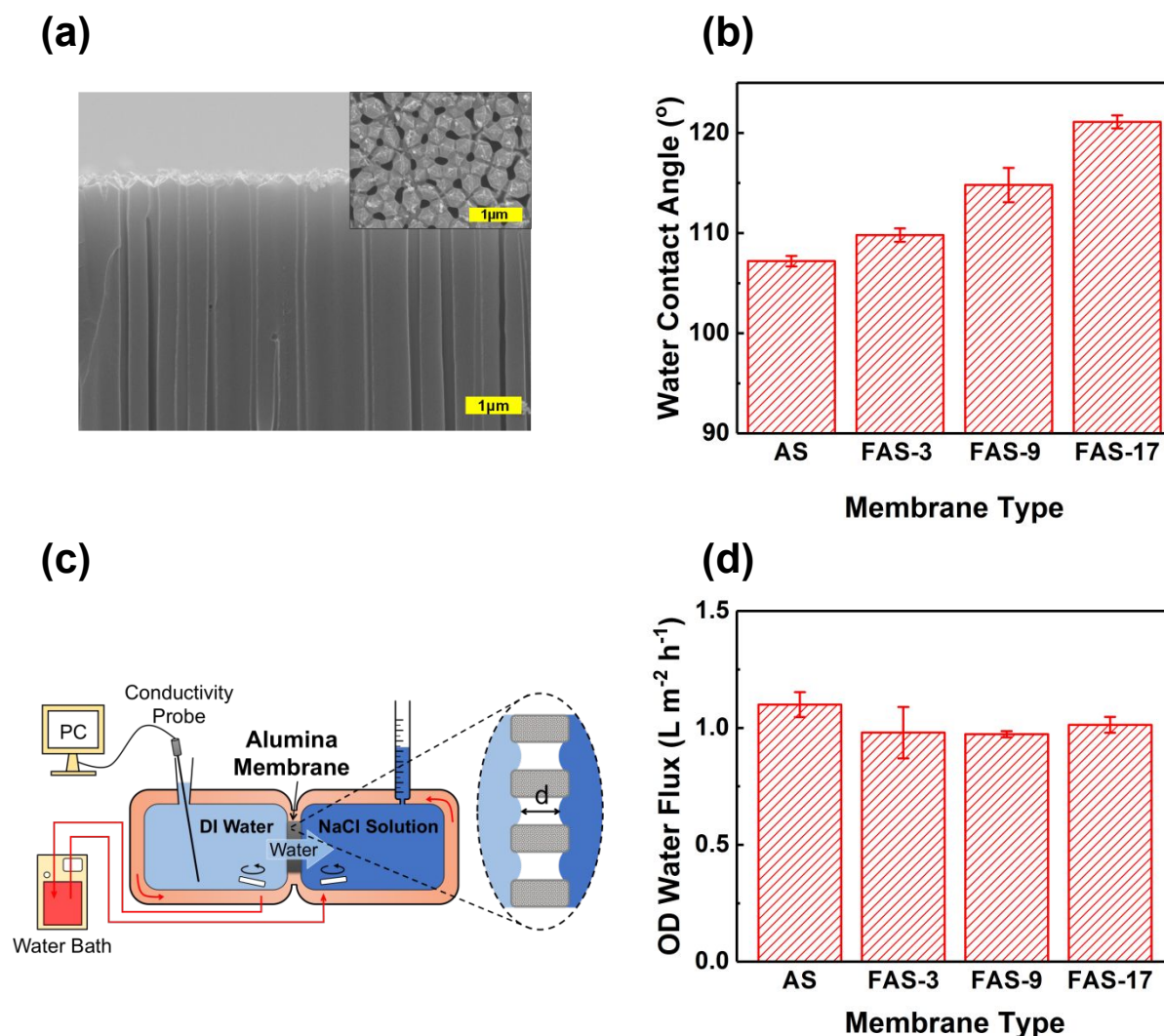
383 **Figure 5.** Optical (left) and fluorescence (right) microscopy images of the cross-sections of (a) FAS-9 QF
 384 membrane and (b) AS QF membrane after the top surfaces of membranes were brought in contact with
 385 Rhodamine B solution with 0.01 mM SDS ($\gamma \approx 66 \text{ mN}\cdot\text{m}^{-1}$). The green strips in the fluorescence
 386 microscope images visualize the penetration depth of the solution into the membrane. The scale bar is 200
 387 μm . Schematics (not drawn to scale) of membrane cross-sections illustrating the degree of liquid-air
 388 interface penetration and the liquid-air interfacial areas for fiber surfaces exhibiting (c) a high wetting
 389 resistance and (d) a low wetting resistance. θ is the local contact angle formed between the fiber surface
 390 and the liquid-air interface ($\theta_1 > \theta_2$).

391

392 **The trade-off between wetting resistance and water vapor flux is absent in the**
 393 **membrane having straight cylindrical pores.** While we employed fibrous membranes in
 394 this study, the trade-off relation between wetting resistance and water vapor flux in DCMD has
 395 also been observed for microporous membranes fabricated by phase inversion (Figure 1). As
 396 illustrated in Figure 5, fibrous or irregular pore structure are proposed to result in the increase of

397 liquid-air interfacial area when the liquid protrudes into membrane pores. If this is the case, we
398 can anticipate that the trade-off relation would not be observed for membranes consisting of
399 straight pores because the liquid-air interfacial areas would vary little even for different wetting
400 resistances as long as pore wetting does not occur.

401 To validate this hypothesis, we employed anodized aluminum oxide (AAO) membranes that
402 comprise cylindrical and straight nanopores with the nominal diameter of 200 nm (Figure 6a).
403 The AAO membranes were hydrophobized by treating them with the four silane molecules (i.e.,
404 AS, FAS-3, FAS-9, and FAS-17). Like the QF membranes, the AAO membrane modified with
405 the silane of a longer fluorocarbon chain was more hydrophobic (Figure 6b). The water vapor
406 flux across the membranes was measured using a bench-scale OD setup (Figure 6c) used in our
407 previous studies.^{40,41} In the OD setup, the feed (distilled water) chamber and the draw (4 M NaCl
408 solution) chamber were separated by the AAO membrane, which were both maintained at the
409 same temperature (40 °C). In the OD process, the driving force of water vapor flow is the water
410 vapor pressure gradient across the membrane created by the osmotic pressure difference between
411 feed and draw. Therefore, OD can be considered as an isothermal variant of MD. The
412 conductivity of feed (distilled water) remained constantly low for all tested membranes, without
413 any occurrence of the membrane pore wetting. As shown in Figure 6d, the water vapor fluxes of
414 AAO membranes modified with the four different silanes did not show significant differences
415 (one-way ANOVA, $F = 3.14$, $p = 0.096$), and no trade-off relation between wetting resistance
416 and water flux was observed. The results of OD experiments substantiate the impact of fibrous or
417 irregular structures that allow liquid-air interfacial area expansion when the wetting resistance is
418 lower.



419 **Figure 6.** (a) Cross-sectional SEM micrograph of the pristine AAO membrane (the inset is the micrograph
 420 of the membrane surface). (b) Static contact angles of water on the surface of the AS, FAS-3, FAS-9, and
 421 FAS-17 AAO membranes. Error bars represent the standard deviations from three different membrane
 422 samples (both left and right contact angles were measured on each sample). (c) Schematic illustration of
 423 the osmotic distillation (OD) experimental setup. (d) OD water vapor fluxes of AS, FAS-3, FAS-9, and
 424 FAS-17 AAO membranes measured by using distilled water at 40 °C as the feed solution and 4 M NaCl
 425 at 40 °C as the draw solution. Error bars represent the standard deviations.

426

427 IMPLICATIONS

428 In this study, we investigated the underlying mechanism for the wettability-flux trade-off relation
 429 in MD using quartz fiber (QF) membranes. We outline potential approaches for minimizing the

430 impact of trade-off relation on attaining high water flux and their limitations. First, decreasing
431 the thickness of a highly wetting-resistant membrane can be a feasible way to reduce the mass
432 transfer resistance of water vapor and thus offset the declined water flux. As previously shown,
433 the penetration of liquid into the membrane pores was marginal even for the membrane having a
434 relatively high surface energy (e.g., AS QF membrane). Fabrication of composite membranes
435 consisting a thin hydrophobic porous layer on a thermally conductive supportive layer would
436 increase the water flux for a given temperature difference.⁴⁸ It should be noted that water flux
437 enhancement by reducing the membrane thickness would be limited by temperature polarization,
438 in particular when the thickness becomes less than $\sim 10 \mu\text{m}$, and also be accompanied by a
439 significant thermal conduction loss.^{49,50}

440 Second, fabricating a membrane that comprises straight pores would not likely exhibit the
441 trade-off relation. Many techniques for fabricating inorganic or polymeric membranes that have
442 cylindrical pores have been explored, including electrochemical processes, selective-etching of
443 block-copolymers, and imprinting.⁵¹⁻⁵³ However, fibrous or irregular pore structures are
444 generally preferred for MD, due to the high porosity and ease of membrane fabrication.
445 Therefore, benefits from the membranes of straight pores with high wetting resistances may not
446 be obvious for MD applications.

447 Third, the membrane surface energy can be tailored to obtain a high water vapor flux if feed
448 water of specific compositions is treated. The surface energy must be determined based on the
449 minimum possible surface tension of the feed water. In such case, a consistent minimum surface
450 tension of the feed water needs to be guaranteed and a rigorous assessment for the risk of
451 potential membrane wetting and the benefit of high water yield will be required.

452

453 ACKNOWLEDGEMENT

454 J.L. acknowledges funding support from the Natural Sciences and Engineering Research Council
455 of Canada (NSERC) through Discovery Grant. T.T acknowledges funding support from
456 Colorado Office of Economic Development and International Trade and CSU Ventures, as well
457 as the Department of Civil and Environmental Engineering, College of Engineering at Colorado
458 State University. A.K.K. acknowledges financial support under award 1751628 from the NSF
459 and under awards R01HL135505 and R21HL139208 from the NIH.

460

461 SUPPORTING INFORMATION

462 Summary of the water flux data of the membrane before and after the surface modification in the
463 literature and the water flux ratios, as well as the corresponding membrane characteristic changes
464 calculated from the data in the literature; Schematic illustration of hydrophobic modification
465 processes; Estimation of capacitance using EIS; Membrane structure characterizations;
466 Measurement of water vapor flux and salt rejection in DCMD experiments; SEM micrographs of
467 the morphologies of FAS-3 QF and FAS-9 QF membranes; Characteristics of modified QF
468 membranes; Water vapor fluxes of the modified QF membranes in DCMD tests; Impedance
469 spectra of AS QF membrane; Estimated capacitances of the modified QF membranes based on
470 the impedance measurements.

471

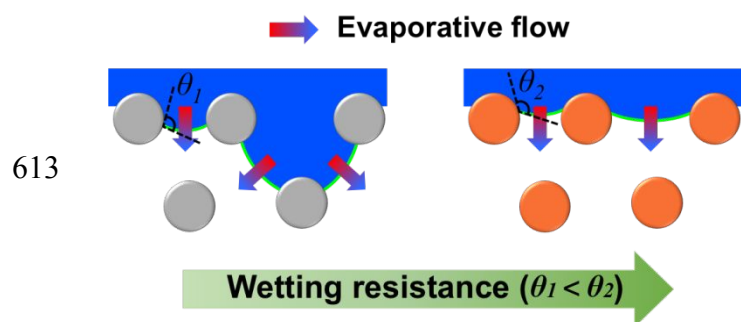
472 REFERENCES

- 473 1. *Wwap (World Water Assessment Programme). The United Nations World Water*
474 *Development Report 4: Managing Water under Uncertainty and Risk*; UNESCO: Paris, 2012.
- 475 2. Ranade, V. V.; Bhandari, V. M., Chapter 1 - Industrial Wastewater Treatment, Recycling,
476 and Reuse: An Overview. In *Industrial Wastewater Treatment, Recycling and Reuse*, Ranade, V.
477 V.; Bhandari, V. M., Eds. Butterworth-Heinemann: Oxford, 2014; pp 1-80.

- 478 3. Tong, T.; Elimelech, M., The Global Rise of Zero Liquid Discharge for Wastewater
479 Management: Drivers, Technologies, and Future Directions. *Environ. Sci. Technol.* **2016**, *50*,
480 6846-6855.
- 481 4. *Wwap (World Water Assessment Programme). the United Nations World Water*
482 *Development Report 2017: Wastewater—the Untapped Resource.* ; UNESCO: Paris, 2017.
- 483 5. Shaffer, D. L.; Arias Chavez, L. H.; Ben-Sasson, M.; Romero-Vargas Castrillón, S.; Yip,
484 N. Y.; Elimelech, M., Desalination and Reuse of High-Salinity Shale Gas Produced Water:
485 Drivers, Technologies, and Future Directions. *Environ. Sci. Technol.* **2013**, *47*, 9569-9583.
- 486 6. Qasim, M.; Badrelzaman, M.; Darwish, N. N.; Darwish, N. A.; Hilal, N., Reverse
487 Osmosis Desalination: A State-of-the-Art Review. *Desalination* **2019**, *459*, 59-104.
- 488 7. Liao, Y.; Wang, R.; Fane, A. G., Engineering Superhydrophobic Surface on
489 Poly(Vinylidene Fluoride) Nanofiber Membranes for Direct Contact Membrane Distillation. *J.*
490 *Membr. Sci.* **2013**, *440*, 77-87.
- 491 8. Boo, C.; Lee, J.; Elimelech, M., Omniphobic Polyvinylidene Fluoride (Pvdf) Membrane
492 for Desalination of Shale Gas Produced Water by Membrane Distillation. *Environ. Sci. Technol.*
493 **2016**, *50*, 12275-12282.
- 494 9. Lee, J.; Boo, C.; Ryu, W.-H.; Taylor, A. D.; Elimelech, M., Development of Omniphobic
495 Desalination Membranes Using a Charged Electrospun Nanofiber Scaffold. *ACS Appl. Mater.*
496 *Interfaces* **2016**, *8*, 11154-11161.
- 497 10. Du, X.; Zhang, Z.; Carlson, K. H.; Lee, J.; Tong, T., Membrane Fouling and Reusability
498 in Membrane Distillation of Shale Oil and Gas Produced Water: Effects of Membrane Surface
499 Wettability. *J. Membr. Sci.* **2018**, *567*, 199-208.
- 500 11. Chew, N. G. P.; Zhao, S.; Malde, C.; Wang, R., Polyvinylidene Fluoride Membrane
501 Modification Via Oxidant-Induced Dopamine Polymerization for Sustainable Direct-Contact
502 Membrane Distillation. *J. Membr. Sci.* **2018**, *563*, 31-42.
- 503 12. Mohammadi Ghaleni, M.; Al Balushi, A.; Kaviani, S.; Tavakoli, E.; Bavarian, M.; Nejati,
504 S., Fabrication of Janus Membranes for Desalination of Oil-Contaminated Saline Water. *ACS*
505 *Appl. Mater. Interfaces* **2018**, *10*, 44871-44879.
- 506 13. Alkhudhiri, A.; Darwish, N.; Hilal, N., Membrane Distillation: A Comprehensive
507 Review. *Desalination* **2012**, *287*, 2-18.
- 508 14. Khayet, M., Membranes and Theoretical Modeling of Membrane Distillation: A Review.
509 *Adv. Colloid Interface Sci.* **2011**, *164*, 56-88.
- 510 15. Rezaei, M.; Warsinger, D. M.; Lienhard V, J. H.; Duke, M. C.; Matsuura, T.; Samhaber,
511 W. M., Wetting Phenomena in Membrane Distillation: Mechanisms, Reversal, and Prevention.
512 *Water Research* **2018**, *139*, 329-352.
- 513 16. Wang, Z.; Chen, Y.; Sun, X.; Duddu, R.; Lin, S., Mechanism of Pore Wetting in
514 Membrane Distillation with Alcohol Vs. Surfactant. *J. Membr. Sci.* **2018**, *559*, 183-195.
- 515 17. Lin, S.; Nejati, S.; Boo, C.; Hu, Y.; Osuji, C. O.; Elimelech, M., Omniphobic Membrane
516 for Robust Membrane Distillation. *Environ. Sci. Technol. Lett.* **2014**, *1*, 443-447.
- 517 18. Liu, T. L.; Kim, C.-J. C., Turning a Surface Superrepellent Even to Completely Wetting
518 Liquids. *Science* **2014**, *346*, 1096-1100.
- 519 19. Lu, K. J.; Zuo, J.; Chang, J.; Kuan, H. N.; Chung, T.-S., Omniphobic Hollow-Fiber
520 Membranes for Vacuum Membrane Distillation. *Environ. Sci. Technol.* **2018**, *52*, 4472-4480.
- 521 20. Li, C.; Li, X.; Du, X.; Tong, T.; Cath, T. Y.; Lee, J., Antiwetting and Antifouling Janus
522 Membrane for Desalination of Saline Oily Wastewater by Membrane Distillation. *ACS Appl.*
523 *Mater. Interfaces* **2019**, *11*, 18456-18465.

- 524 21. McGaughey, A. L.; Karandikar, P.; Gupta, M.; Childress, A. E., Hydrophobicity Versus
525 Pore Size: Polymer Coatings to Improve Membrane Wetting Resistance for Membrane
526 Distillation. *ACS Appl. Polym. Mater.* **2020**, *2*, 1256-1267.
- 527 22. Li, X.; Dutta, A.; Dong, Q.; Rollings-Scattergood, S.; Lee, J., Dissolved Methane
528 Harvesting Using Omniphobic Membranes for Anaerobically Treated Wastewaters. *Environ. Sci.*
529 *Technol. Lett.* **2019**, *6*, 228-234.
- 530 23. Huang, Y. X.; Wang, Z.; Jin, J.; Lin, S., Novel Janus Membrane for Membrane
531 Distillation with Simultaneous Fouling and Wetting Resistance. *Environ Sci Technol* **2017**, *51*,
532 13304-13310.
- 533 24. An, X.; Liu, Z.; Hu, Y., Amphiphobic Surface Modification of Electrospun Nanofibrous
534 Membranes for Anti-Wetting Performance in Membrane Distillation. *Desalination* **2018**, *432*,
535 23-31.
- 536 25. Lu, C.; Su, C.; Cao, H.; Ma, X.; Duan, F.; Chang, J.; Li, Y., F-Poss Based Omniphobic
537 Membrane for Robust Membrane Distillation. *Materials Letters* **2018**, *228*, 85-88.
- 538 26. Lu, X.; Peng, Y.; Qiu, H.; Liu, X.; Ge, L., Anti-Fouling Membranes by Manipulating
539 Surface Wettability and Their Anti-Fouling Mechanism. *Desalination* **2017**, *413*, 127-135.
- 540 27. Woo, Y. C.; Kim, Y.; Yao, M.; Tijing, L. D.; Choi, J. S.; Lee, S.; Kim, S. H.; Shon, H.
541 K., Hierarchical Composite Membranes with Robust Omniphobic Surface Using Layer-by-Layer
542 Assembly Technique. *Environ. Sci. Technol.* **2018**, *52*, 2186-2196.
- 543 28. Zheng, R.; Chen, Y.; Wang, J.; Song, J.; Li, X.-M.; He, T., Preparation of Omniphobic
544 PvdF Membrane with Hierarchical Structure for Treating Saline Oily Wastewater Using Direct
545 Contact Membrane Distillation. *J. Membr. Sci.* **2018**, *555*, 197-205.
- 546 29. Wang, M.; Liu, G.; Yu, H.; Lee, S.-H.; Wang, L.; Zheng, J.; Wang, T.; Yun, Y.; Lee, J.
547 K., ZnO Nanorod Array Modified PvdF Membrane with Superhydrophobic Surface for Vacuum
548 Membrane Distillation Application. *ACS Appl. Mater. Interfaces* **2018**, *10*, 13452-13461.
- 549 30. Karanikola, V.; Boo, C.; Rolf, J.; Elimelech, M., Engineered Slippery Surface to Mitigate
550 Gypsum Scaling in Membrane Distillation for Treatment of Hypersaline Industrial Wastewaters.
551 *Environ. Sci. Technol.* **2018**, *52*, 14362-14370.
- 552 31. Wang, W.; Du, X.; Vahabi, H.; Zhao, S.; Yin, Y.; Kota, A. K.; Tong, T., Trade-Off in
553 Membrane Distillation with Monolithic Omniphobic Membranes. *Nat. Commun.* **2019**, *10*, 3220.
- 554 32. Chen, Y.; Lu, K. J.; Chung, T.-S., An Omniphobic Slippery Membrane with
555 Simultaneous Anti-Wetting and Anti-Scaling Properties for Robust Membrane Distillation. *J.*
556 *Membr. Sci.* **2020**, *595*, 117572.
- 557 33. Chul Woo, Y.; Chen, Y.; Tijing, L. D.; Phuntsho, S.; He, T.; Choi, J.-S.; Kim, S.-H.;
558 Kyong Shon, H., CF₄ Plasma-Modified Omniphobic Electrospun Nanofiber Membrane for
559 Produced Water Brine Treatment by Membrane Distillation. *J. Membr. Sci.* **2017**, *529*, 234-242.
- 560 34. Guo, J.; Deka, B. J.; Kim, K.-J.; An, A. K., Regeneration of Superhydrophobic TiO₂
561 Electrospun Membranes in Seawater Desalination by Water Flushing in Membrane Distillation.
562 *Desalination* **2019**, *468*, 114054.
- 563 35. Chen, Y.; Tian, M.; Li, X.; Wang, Y.; An, A. K.; Fang, J.; He, T., Anti-Wetting Behavior
564 of Negatively Charged Superhydrophobic PvdF Membranes in Direct Contact Membrane
565 Distillation of Emulsified Wastewaters. *J. Membr. Sci.* **2017**, *535*, 230-238.
- 566 36. Palacio, L.; Prádanos, P.; Calvo, J. I.; Hernández, A., Porosity Measurements by a Gas
567 Penetration Method and Other Techniques Applied to Membrane Characterization. *Thin Solid*
568 *Films* **1999**, *348*, 22-29.

- 569 37. Wu, S., Calculation of Interfacial Tension in Polymer Systems. *J. polym. sci., Polym.*
570 *symp.* **1971**, *34*, 19-30.
- 571 38. Müller, M.; Oehr, C., Comments on “an Essay on Contact Angle Measurements” by
572 Strobel and Lyons. *PLASMA PROCESS POLYM* **2011**, *8*, 19-24.
- 573 39. Boo, C.; Lee, J.; Elimelech, M., Engineering Surface Energy and Nanostructure of
574 Microporous Films for Expanded Membrane Distillation Applications. *Environ Sci Technol*
575 **2016**, *50*, 8112-8119.
- 576 40. Lee, J.; Laoui, T.; Karnik, R., Nanofluidic Transport Governed by the Liquid/Vapour
577 Interface. *Nat. Nanotechnol.* **2014**, *9*, 317-323.
- 578 41. Lee, J.; Straub, A. P.; Elimelech, M., Vapor-Gap Membranes for Highly Selective
579 Osmotically Driven Desalination. *J. Membr. Sci.* **2018**, *555*, 407-417.
- 580 42. Chen, Y.; Wang, Z.; Jennings, G. K.; Lin, S., Probing Pore Wetting in Membrane
581 Distillation Using Impedance: Early Detection and Mechanism of Surfactant-Induced Wetting.
582 *Environ. Sci. Technol. Lett.* **2017**, *4*, 505-510.
- 583 43. Huang, Q.; Luo, Q.; Chen, Z.; Yao, L.; Fu, P.; Lin, Z., The Effect of Electrolyte
584 Concentration on Electrochemical Impedance for Evaluating Polysulfone Membranes. *Environ.*
585 *Sci. Water Res. Technol.* **2018**, *4*, 1145-1151.
- 586 44. Wang, D.; Dang, Z.-M., 12 - Processing of Polymeric Dielectrics for High Energy
587 Density Capacitors. In *Dielectric Polymer Materials for High-Density Energy Storage*, Dang, Z.-
588 M., Ed. William Andrew Publishing: 2018; pp 429-446.
- 589 45. Matijević, E.; Pethica, B. A., The Properties of Ionized Monolayers. Part 1.—Sodium
590 Dodecyl Sulphate at the Air/Water Interface. *Trans. Faraday Soc.* **1958**, *54*, 1382-1389.
- 591 46. Tuteja, A.; Choi, W.; Ma, M. L.; Mabry, J. M.; Mazzella, S. A.; Rutledge, G. C.;
592 McKinley, G. H.; Cohen, R. E., Designing Superoleophobic Surfaces. *Science* **2007**, *318*, 1618-
593 1622.
- 594 47. Zhao, H.; Park, K.-C.; Law, K.-Y., Effect of Surface Texturing on Superoleophobicity,
595 Contact Angle Hysteresis, and “Robustness”. *Langmuir* **2012**, *28*, 14925-14934.
- 596 48. Su, M.; Teoh, M. M.; Wang, K. Y.; Su, J.; Chung, T.-S., Effect of Inner-Layer Thermal
597 Conductivity on Flux Enhancement of Dual-Layer Hollow Fiber Membranes in Direct Contact
598 Membrane Distillation. *J. Membr. Sci.* **2010**, *364*, 278-289.
- 599 49. Deshmukh, A.; Lee, J., Membrane Desalination Performance Governed by Molecular
600 Reflection at the Liquid-Vapor Interface. *Int. J. Heat Mass Transfer* **2019**, *140*, 1006-1022.
- 601 50. Drioli, E.; Ali, A.; Macedonio, F., Membrane Distillation: Recent Developments and
602 Perspectives. *Desalination* **2015**, *356*, 56-84.
- 603 51. Belwalkar, A.; Grasing, E.; Van Geertruyden, W.; Huang, Z.; Misiolek, W. Z., Effect of
604 Processing Parameters on Pore Structure and Thickness of Anodic Aluminum Oxide (Aao)
605 Tubular Membranes. *J. Membr. Sci.* **2008**, *319*, 192-198.
- 606 52. Abetz, V., Isoporous Block Copolymer Membranes. *Macromol. Rapid Commun.* **2015**,
607 *36*, 10-22.
- 608 53. Zhan, Z.; Lei, Y., Sub-100-Nm Nanoparticle Arrays with Perfect Ordering and Tunable
609 and Uniform Dimensions Fabricated by Combining Nanoimprinting with Ultrathin Alumina
610 Membrane Technique. *ACS Nano* **2014**, *8*, 3862-3868.
- 611

612 **TABLE OF CONTENTS**

614